Available online at www.sciencedirect.com
ScienceDirect
Journal of Bionic Engineering 11 (2014) 610–619

Biocompatible DCPD Coating Formed on AZ91D Magnesium Alloy by Chemical Deposition and Its Corrosion Behaviors in SBF

Zhongji Cheng, Jianshe Lian, Yanxian Hui, Guangyu Li

Key Laboratory of Automobile Materials (*Ministry of Education of China*), *College of Materials Science and Engineering*, *Jilin University*, *Changchun* 130022, *P. R. China*

Abstract

Bioactive calcium phosphate coatings were prepared on AZ91D magnesium alloy in phosphating solution in order to improve the corrosion resistance of the magnesium alloy in Simulated Body Fluid (SBF). The surface morphologies and compositions of the calcium phosphate coatings deposited in the phosphating bath with different compositions were investigated by Scanning Electron Microscopy (SEM) with Energy Dispersive Spectrometer (EDS) and X-ray Diffraction (XRD). Results showed that the calcium phosphate coating was mainly composed of dicalcium phosphate dihydrate (CaHPO4•2H2O, DCPD), with Ca/P ratio of approximately 1:1. The corrosion resistance was evaluated by acid drop, electrochemical polarization, electrochemical impedance spectroscopy and immersion tests. The dense and uniform calcium phosphate coating obtained from the optimal phosphating bath can greatly decrease the corrosion rate and hydrogen evolution rate of AZ91D magnesium alloy in SBF.

Keywords: DCPD coating, chemical deposited method, magnesium alloy, corrosion rate, SBF

doi: 10.1016/S1672-6529(14)60072-X

1 Introduction

As potential biodegradable implant materials, magnesium and its alloys have attracted more and more attentions due to their proper mechanical properties and good biocompatibilities[1–9]. Mg ion is the 4th major cation in human serum[10]. Mg ion is one of the elements that are essential to human metabolism, and it can be naturally found in bone tissue[11]. In human body, approximately two-thirds of total magnesium ions are in bone, one-thirds in tissue sections and only approximately 1%~2% in extracellular fluid[12]. The deficiency of magnesium in human body may cause bone strength reduction and osteoporosis[13–14]. Moreover, magnesium as light metal is widely used in engineering. The density of magnesium (1.74 g·cm^{-3} – 2.0 g·cm^{-3}) is very close to the density of natural bone (1.8 g·cm^{-3} – 2.1 g·cm^{-3}). Compared to other metallic biomaterials, magnesium has a low elastic modulus of 45 GPa, and it is much lower than that of titanium (110 GPa), stainless steel (200 GPa) and cobalt chromium (210 GPa). As a result, stress shielding effect during bone transplanting operation can be largely reduced or avoided when magnesium is employed as an implant. However, fast corrosion rate of magnesium and its alloys in human body environment limits their potential uses as medical implant materials[15–17]. It is necessary to improve the corrosion resistance of magnesium alloys in human body environment.

Dicalcium phosphate dihydrate (CaHPO4•2H2O, DCPD) with excellent biocompatibility and osteoconductive properties was widely used as biomedical materials[18–21]. DCPD coating has a low solubility in human body fluid or blood plasma, due to its chemical and structural similarities with natural bone[22]. For this reason, many approaches have already been developed to obtain DCPD coating on magnesium alloy for orthopedic use, such as anodic oxidation[23], electroless plating[24], biomimetic approach[25,26], and chemical conversion coating[27–33]. Moreover, some pre-treatments or post-treatments were taken to improve the performance of DCPD. In Ref. [34], surface treatment (shot peening, SP) was used before DCPD electrochemically deposited on AZ31 alloy. The results showed that SP significantly increased the surface hardness of AZ31comparing with

Corresponding author: Guangyu Li
E-mail: guangyu@jlu.edu.cn

grinded surface, but SP decreased the corrosion resistance of AZ31. In Ref.[35], hydrothermal treatment of Micro-Arc Oxide (MAO) layer on AZ31 magnesium alloy at 150 ˚C was performed to obtain DCPD, and this method improved the corrosion resistance of magnesium alloys in SBF, especially the pitting corrosion resistance. In Ref. [36], DCPD coating was firstly deposited on the substrate surface of AZ91D magnesium alloy, and then being immersed in Simulated Body Fluid (SBF) to obtain the hydroxyapatite (HA) coating with better corrosion resistance, but this two-step deposition method is complicated and expensive. Among these approaches, the chemical methods have lower cost and are easy to be operated, and the structure of coating formed in solution is much more similar to that of the bone mineral[37]. Compared to other magnesium alloys, AZ91D magnesium alloy has a higher Al content with good mechanical properties and corrosion resistance, so it can be proper candidate as biomedical materials[2–3,38].

In this study, a DCPD coating on AZ91D magnesium alloy was prepared by chemical deposition in a phosphating bath. By adjusting the phosphating bath, a uniform and dense coating was obtained, and its corrosion behaviors in SBF were experimentally investigated.

2 Materials and methods

2.1 Sample preparation

AZ91D die cast magnesium alloy was used in our experiments as substrate material, and the sample size is 20 mm × 20 mm × 3 mm. Table 1 shows the chemical compositions of AZ91D alloy.

Table 1 Chemical compositions of AZ91D magnesium alloy (in wt%)

Compositions	Percentage (wt%)
Al	8.77
Zn	0.74
Mn	0.18
Cu	0.01
Ni	0.01
Fe	0.01
Si	≤ 0.10
Ca	≤ 0.10
K	≤ 0.10
Mg	Balance

2.2 Phosphating process and acid drop test

Table 2 shows the composition of phosphating bath and all operation parameters for DCPD deposition on the surface of AZ91D magnesium alloy. All reagents used in our experiments were analytical grade produced by Tianjin Guangfu Fine Chemical Research Institute. The pH value of the bath was adjusted by H_3PO_4 or NaOH. By adjusting the composition and pH value of phosphating bath, a dense and uniform coating on magnesium substrate was prepared.

Acid drop test was employed to quickly evaluate the corrosion resistance of the coatings formed on magnesium substrate. The test in potassium chlorate plus hydrofluoric acid solution at room temperature was performed for different coatings formed on AZ91D magnesium alloy surface. Once a drop of self-made solution was dropped in certain circular area on the alloy surface started to timing, the time was recorded when the solution fades to colorless from the original red color. The experiments on each coating were repeated three times, and the average value of the three results was considered as the corrosion time.

2.3 Electrochemical test

To determine the optimal pH value of phosphating bath, polarization test in a 3 wt% NaCl aqueous solution was employed to judge the quality of coatings obtained under different pH value. Polarization test and Electrochemical Impedance Spectroscopy (EIS) in SBF were performed to evaluate the corrosion resistance of DCPD on AZ91D magnesium alloy. Polarization test and EIS

Table 2 Compositions and operating conditions of DCPD coated on AZ91D magnesium alloy (Samples were cleaned with deionized water as quickly as possible between any two process of the treatments.)

Steps	Operation	Bath compositions	Conditions
1	Grinding	No. 300~1500 SiC sandpaper	
2	Alkaline cleaning	NaOH 45 g·L^{-1} $Na_3PO_4{\cdot}12H_2O$ 10 g·L^{-1}	20 min, 65 ˚C
3	Phosphating	H_3PO_4 60 mL·L^{-1} CaO 10 g·L^{-1} $Ca(NO_3)_2$ 10 g·L^{-1} $C_6H_4O_5NSNa$ 1~4g Na_2MoO_4 1~2 g·L^{-1}	30–40 min, 40 ˚C, pH = 2.5–3.5
4	Dryness		40 ˚C, 10 min

were carried out on an Electrochemical Workstation (Lanlike, Tianjin, China) by linear sweep voltammeter technique, and a conventional three-electrode cell with platinum was used as counter electrode, with Saturated Calomel Electrode (SCE, +0.242 V vs. SHE) as reference electrode and the samples were used as working electrode. The EIS test was performed in a frequency range from 100 mHz to 100 kHz under the Open-Circuit Potential (OCP) values. The applied alternating potential had root mean square amplitude of 10 mV on the OCP. The obtained impedance data were expressed by Nyquist plot. The coated samples were covered by epoxy resin (EP651) and only the coating area of 1 × 1 cm^2 was exposed to the electrolyte. After a stabilization period of 30 min in the solution to stabilize the OCP, the polarization test and EIS were performed at a scan rate of 5 $mV \cdot s^{-1}$. For comparison, the bare magnesium alloys were also tested.

2.4 Immersion in SBF

The protection capacity and biodegradable characteristics of the coating were evaluated by electrochemical tests and immersion test in SBF at 37±1 ˚C. SBF was composed of 8 $g \cdot L^{-1}$ NaCl, 0.185 $g \cdot L^{-1}$ $CaCl_2$, 0.4 $g \cdot L^{-1}$ KCl, 0.06 $g \cdot L^{-1}$ KH_2PO_4, 0.1 $g \cdot L^{-1}$ $MgSO_4 \cdot 7H_2O$, 0.35 $g \cdot L^{-1}$ $NaHCO_3$, 0.48 $g \cdot L^{-1}$ Na_2HPO4, and 1 $g \cdot L^{-1}$ $C_6H_6O_6$(glucose)[23–25], and its pH value was adjusted to a physiological pH value of 7.4 with HCl and $(CH_2OH)CNH_2$.

To evaluate the *in vitro* degradability and corrosion rate, an inverted measuring cylinder was used to collect the volumes of hydrogen evolution of AZ91D magnesium alloy in SBF. A beaker containing 250 mL SBF was used for samples immersion test at 37 ˚C. The SBF was not refreshed during the immersion test.

The coated samples were immersed in SBF for 7 d. After that the samples were taken from the SBF, and then rinsed with deionized water and dried at 40 ˚C. Then Fourier-Transformed Infrared Spectroscopy (FTIR) (Avatar 370, Nicolet, America) was employed to detect the surface functional groups. The mode of transmission was collected at room temperature and potassium bromide (KBr) as blank ground. The scanning rate is in the range between 4000 cm^{-1} and 400 cm^{-1}.

2.5 Microstructure characterization

The surface morphologies of coated samples were investigated by a Scanning Electron Microscopy (SEM) (JSM-5310, Japan Electronics), equipped with Energy-Disperse Spectrometer (EDS). The chemical composition of phosphate coating was observed by an XRD (Rigaku Dymax,103 Japan) with a Cu Kα radiation (λ = 0.154178 nm).

3 Results and discussion

3.1 Morphologyies of coatings formed in different phosphating baths

In present phosphating bath, $C_6H_4O_5NSNa$ and Na_2MoO_4 were used as accelerator to form a dense and uniform coating. For high chemical reactivity of magnesium alloy, pH value of phosphating bath is crucial to obtain a high quality phosphate coating. By adjusting the amount of $C_6H_4O_5NSNa$ and Na_2MoO_4, and pH value, the optimal composition of phosphating bath was found. The surface morphologies of the phosphate coatings formed on AZ91D magnesium alloy surface in different phosphating baths were shown in Fig. 1.

It was found that the addition of $C_6H_4O_5NSNa$ will evidently affect the morphologies of phosphate coatings. $C_6H_4O_5NSNa$ can provide more sites for nucleation and growth of phosphate crystals, so it is helpful to form an integrated phosphate film. It can be seen from Fig. 1,with the increase in the content of $C_6H_4O_5NSNa$, the coatings formed on the surface successively composed of buck-shaped crystals (Fig. 1a), bar-shaped crystals (Fig. 1b), and flower-like crystals (Figs. 1c and 1d).

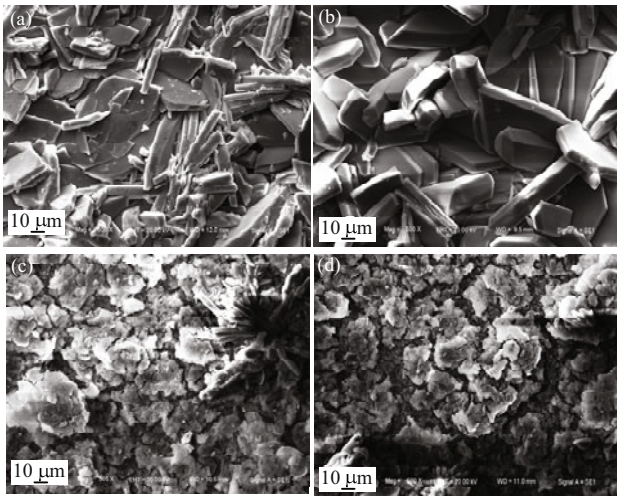

Fig. 1 The surface morphologies of AZ91D magnesium alloy after treating in phosphating baths with (a) 0 g, (b) 1 g, (c) 2 g and (d) 4 g $C_6H_4O_5NSNa$, respectively.

Fig. 2 shows that the addition of Na_2MoO_4 also has a great influence on the morphologies of phosphate coatings. In the acid phosphating bath, molybdate ion (MoO_4^{2-}) reacted with magnesium ion (Mg^{2+}) to form magnesium molybdate ($MgMoO_4$), resulting in the addition of more sites for the nucleation and growth of phosphate crystals. So a more dense phosphate coating was formed as bar-shape phosphate crystals became small (Figs. 2a and 2b). However, with the increase in the content of Na_2MoO_4, molybdate ion (MoO_4^{2-}) reacted with calcium ion (Ca^{2+}) to form indissoluble calcium molybdate ($CaMoO_4$), resulting in an adverse effect on the formation of phosphate coating (Figs. 2c and 2d).

Fig. 3 shows that pH value of phosphating baths has a great influence on the morphologies of phosphate coatings. Under the condition of pH = 2.5, magnesium alloy substrate was corroded rapidly, producing a large amount of hydrogen. Meanwhile, the deposition reaction happened faster than the dissolution reaction, so an incomplete coating was formed on the substrate surface (Fig. 3a). Under the condition of pH = 3.0, a dense and uniform coating was formed on the substrate surface (Fig. 3b). But with the increase in pH value, a porous coating was formed resulted from too lager phosphate-crystals (Fig. 3c).

To quickly evaluate the corrosion resistance of above-mentioned coatings, acid drop tests were carried out, and corresponding results were shown in Fig. 4. The shortest corrosion time of coated samples (1688 s) was far longer than that of bare AZ91D alloy (3 s). Both the optimal amount of $C_6H_4O_5NSNa$ and Na_2MoO_4 are 1 g, and optimal pH value of the bath is 3.0. Fig. 5 shows the morphology of coating formed in optimal phosphating bath, indicating less than 10 μm bar-shaped crystals distributed uniformly on the surface.

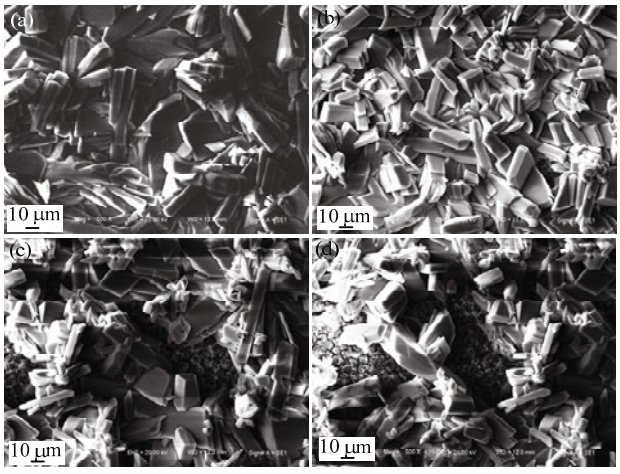

Fig. 2 The surface morphologies of AZ91D magnesium alloy after treating in phosphating baths with (a) 0 g, (b) 1 g, (c) 1.5 g and (d) 2 g Na_2MoO_4, respectively.

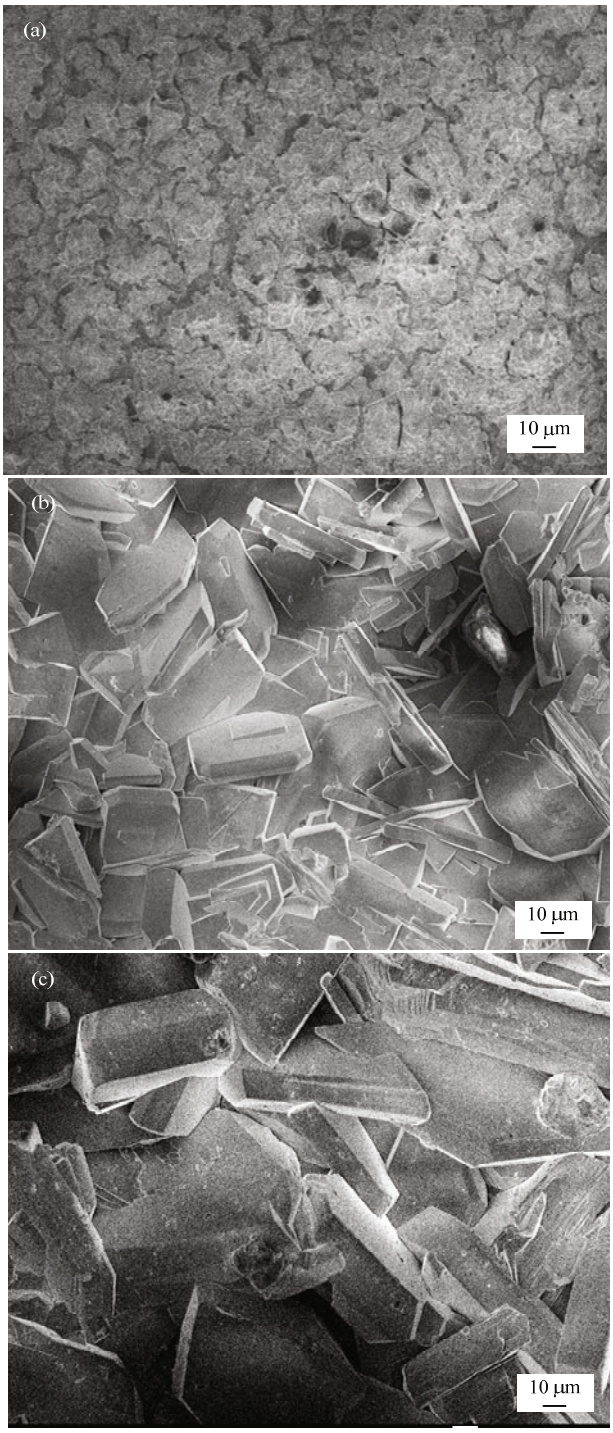

Fig. 3 The surface morphologies of AZ91D magnesium alloy after treating in phosphating baths with (a) pH = 2.5, (b) pH = 3.0, (c) pH = 3.5, respectively.

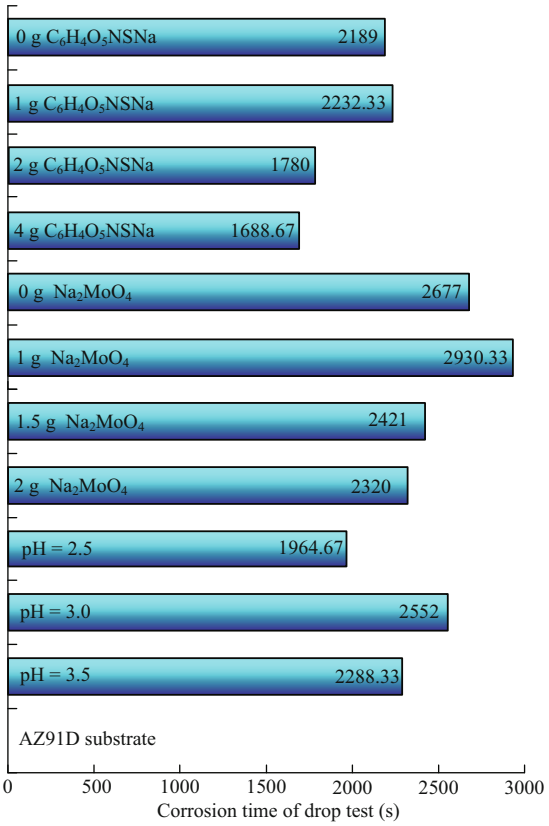

Fig. 4 Corrosion time for coatings formed in different phosphating baths by acid drop test.

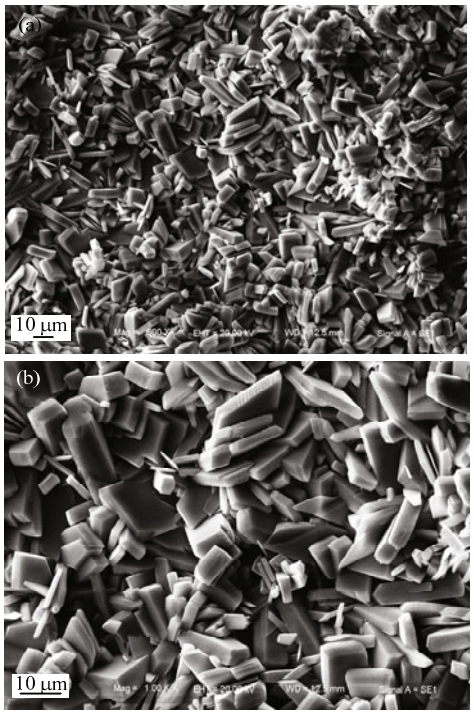

Fig. 5 The surface morphologies AZ91D magnesium alloy after treating in optimal phosphating bath composed of CaO = 10 g·L^{-1}, H_3PO_4 = 60 mL·L^{-1}, $Ca(NO_3)_2$ = 10 g·L^{-1}, Na_2MoO_4 = 1 g·L^{-1}, $C_6H_4O_5NSNa$ = 1 g·L^{-1}, pH = 3.0.

3.2 Microstructure and deposition reactions of the coating

Fig. 6a shows the high magnification of Fig. 5, indicating that magnesium alloy substrate is completely covered with random distributed bar-shaped crystals of 10–20 μm in length and 2–3 μm in thickness. Fig. 6b shows the EDS analysis carried out on the coating, the result indicates that the coating is mainly composed of O, P, Ca, and Mg, and the Mg content is 2.33 wt% (mass friction). XRD was carried out on the coating to study its phase constitution, as shown in Fig. 7. XRD result shows that well crystallized dicalcium phosphate dihydrate ($CaHPO_4·2H_2O$, DCPD) was formed on the magnesium alloy substrate, and small magnesium peaks were detected. According to the microstructure and phase of the coating as well as the bath composition, the deposition reactions of coating can be deduced.

During phosphating process, CaO and H_3PO_4 are the main substance of coating in the bath. So, the reaction between CaO and H_3PO_4 is

$$CaO + 2H_3PO_4 \rightarrow Ca^{2+} + 2H_2PO_4^- + H_2O, \quad (1)$$

then the reduction reaction of $H_2PO_4^-$ occurs:

$$2H_2PO^- + 2e^- \rightarrow 2HPO_4^{2-} + H_2\uparrow. \quad (2)$$

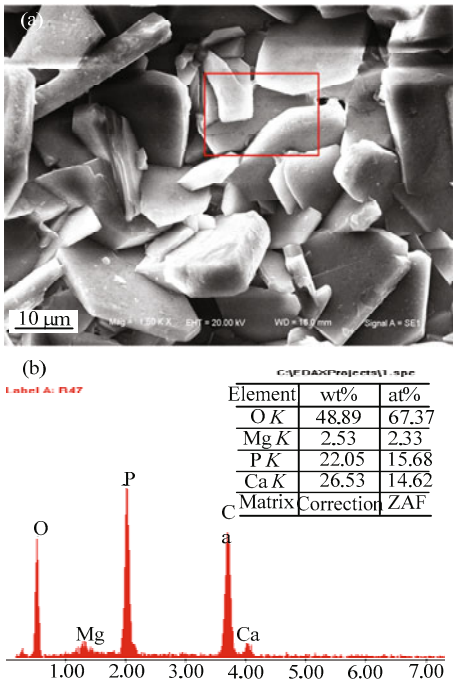

Fig. 6 The surface morphology chemically coated AZ91D magnesium alloy in optimal phosphating bath (a) higher magnification of Fig. 5; (b) EDS of the zone in (a).

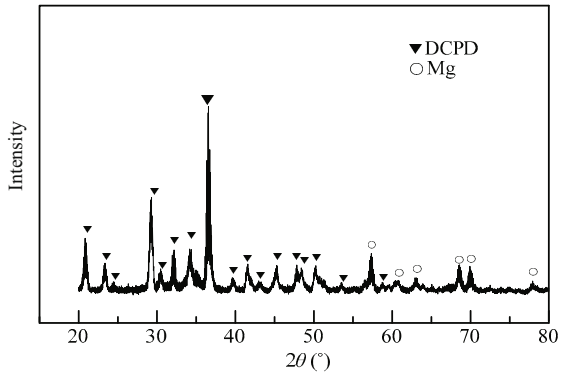

Fig. 7 XRD pattern of AZ91D alloy with the coating.

The HPO_4^{2-} produced by Eq. (2) can react with Ca^{2+} to form the desired $CaHPO_4{\cdot}2H_2O$ (DCPD):

$$Ca^{2+}+HPO_4^{2-}+2H_2O \rightarrow CaHPO_4+2H_2O. \quad (3)$$

3.3 Electrochemical test

To study the corrosion behaviors of the DCPD coating on AZ91D magnesium alloy, electrochemical tests were conducted on the coated samples, as shown in Figs. 7 and 8, where a more positive potential and lower anodic current density was clearly shown for the samples coated with DCPD coatings. The corrosion potential (E_{corr}) and corrosion current density (I_{corr}) obtained in this experiment were compared with those of several calcium phosphate coatings in references (Table 3). From Table 3 we can see that E_{corr} of this paper is the most postive one in both solutions, showing that our prepared DCPD coatings can enhance the corrosion resistance behaviors of the samples in both 3 wt% NaCl solution and SBF. However, no obvious decrease in the corrosion rate has been observed because the values of I_{corr} of our prepared DCPD coatings are still in the range of 0.26–30 $\mu A{\cdot}cm^{-2}$.

The degradation process of AZ91D magnesium alloy in SBF was analyzed based on EIS (Fig. 9). For all samples the Nyquist plots obtained show two time constants, corresponding to the characteristics of solution/coating interface and solution/substrate interface, respectively[39]. The curves of the coatings contain two capacitive loops without the inductive loop, and the loop dimension of the coated alloys increased obviously in comparison with that of bare alloy. It is well known that the bigger the diameter of the semicircle the better the corrosion resistance of the sample[34]. In Fig. 9, the coated samples show larger semicircles as compared with uncoated samples, showing that the DCPD coating formed on the substrate can improve the corrosion resistance of AZ91D alloy in SBF.

Table 3 Comparison of electrochemical parameters among different calcium phosphate coatings

Substrate/Reference	Corrosive medium	E_{corr} (V *vs*.SCE)	I_{corr} ($\mu A{\cdot}m^{-2}$)
AZ91D in this paper	3.0wt%NaCl	−1.27	3.2
AZ91D in this paper	SBF	−1.26	0.32
AZ91D in Ref.[36]	SBF	−1.523	2.6
Mg in Ref.[40]	3.5wt%NaCl	−1.65	0.28
AZ91D in Ref.[41]	SBF	−1.51	30
Mg-Zn-Ca in Ref.[42]	SBF	−1.41	25

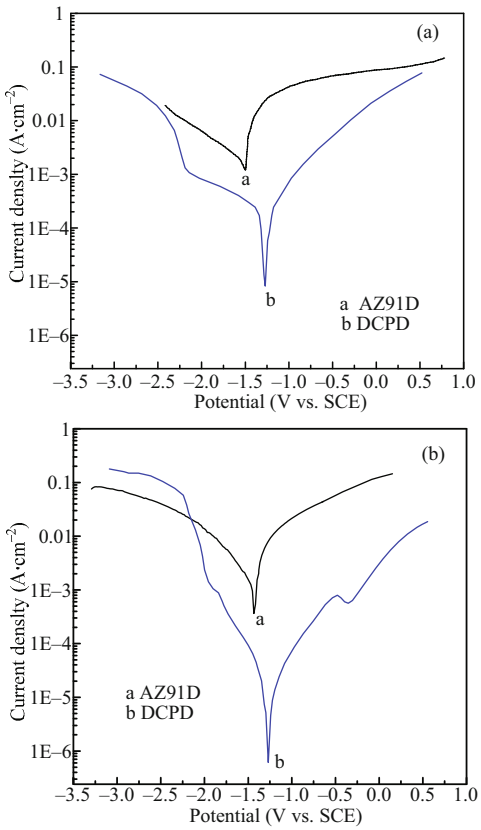

Fig. 8 Electrochemical polarization curves of AZ91D magnesium alloy: (a) in 3 wt% NaCl solution and (b) in SBF.

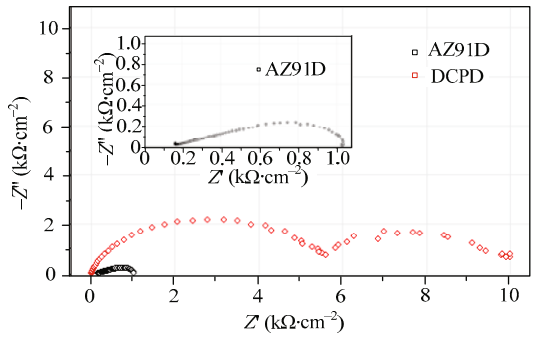

Fig. 9 EIS of uncoated and coated AZ91D magnesium alloys in SBF.

3.4 Immersion in SBF

Hydrogen evolution is always happened during the corrosion of magnesium alloy[43–44], so the hydrogen evolution of the coated AZ91D magnesium alloy in SBF can be used to estimate the corrosion resistance[18,45–47]. The rates of hydrogen evolution in uncoated and coated AZ91D magnesium alloys in SBF at 37 ˚C were shown in Fig. 10. For uncoated sample, the rate of hydrogen evolution increases obviously during the first 4d immersion and gradually reaches its maximal value of 44.2 $mL \cdot cm^2 \cdot d^{-1}$ during the follow-up immersion, which indicates that the corrosion rate of the uncoated sample increases quickly. In contrast to uncoated sample, a very low rate of hydrogen evolution less than 5.8 $mL \cdot cm^2 \cdot d^{-1}$ was observed for the coated sample during SBF immersion for the tested period of seven days. In Ref. [18], the value of hydrogen evolution is approximately 9.0 $mL \cdot cm^2 \cdot d^{-1}$, which is more higher than that of the result in this paper, indicating that the DCPD coating obtained in this paper can significantly slow down the corrosion rate of magnesium alloy in SBF.

The surface morphology and the FTIR spectrum of the DCPD coating after 7d immersion in SBF were shown in Fig. 11. Although some bar-shaped crystals may have dissolved in the SBF, there was no obvious corrosion of the DCPD coating. According to the FTIR spectrum shown in Fig. 11b, the broad absorption band at 3430 cm^{-1} is attributed to the stretching vibration of the OH group. The broad absorption band at 1640 cm^{-1} is caused by H_2O, because both the sample and the KBr powder may absorb H_2O. Absorption bands at 862 cm^{-1} could be confirmed to be the typical peak of PO_4 group. The bands at 1046 cm^{-1} and 570 cm^{-1} are responsible for PO_4 group. The bands at 1430 $cm^{-1}$and 862 cm^{-1} are associated with carbonates. The appearance of carbonates indicates that the composition variation of the coating is mainly carbonated hydroxyapatite. The DCPD coating first dissolved in SBF solution and then mineralized[48]. In SBF, the dissolution mechanism of Ca ion and P ion is mainly dominated by ion exchange[48], and the mineralization is driven by electrostatic interaction of negative surface-charged groups with ions in the fluid[49–50]. Carbonated hydroxyapatite ($Ca_{10}(PO_4)_6(OH)_2$) with lower crystallinity generates the inorganic composition of bone (bone mineral)[51]. This reveals the DCPD coating is bioactive and osteoconductive in SBF[52].

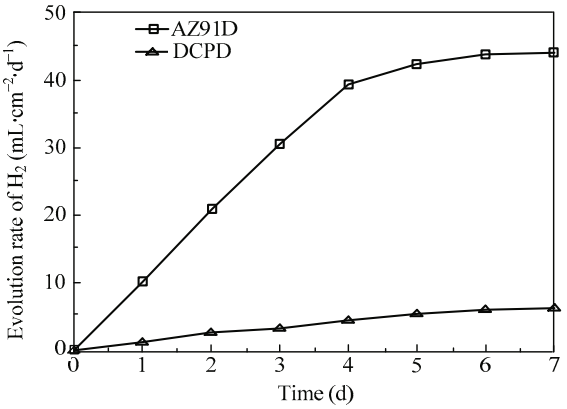

Fig. 10 Hydrogen evolution rate of bare and coated AZ91D magnesium alloys in SBF at 37 ˚C.

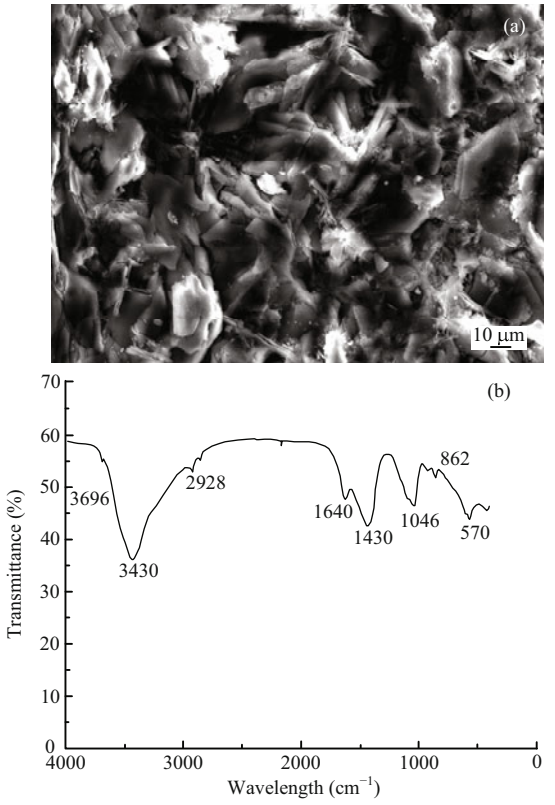

Fig. 11 (a) SEM image of surface morphology of DCPD coating after 7d immersion in SBF and (b) FT-IR spectra.

During 7d immersion in SBF, the whole process of the chemically coated AZ91D magnesium alloy can be divided into three stages according to the dissolution-precipitation dynamic balance in SBF[33].

Firstly, from the beginning of immersion to the 3rd day, the dominant reaction is the dissolution of coating. In the solution, P ions is binding to free Ca ions to form apatite, so more and more P ions was consumed with the increase in immersion time. Secondly, from the 4th day

to the 5th day, the dissolution-precipitation balance is changed, and the dominant reaction is the precipitation of coating. With the increase in immersion time, the concentrations of Ca and P ions decreased, because their consumptions are faster than the supply by dissolution. Thirdly, after 5th day, with the formation of bone-like apatite, Ca_{10}–x$(PO_4)_6$–x(CO_3)x$(OH)_2$, the concentration of P ions increased because of a part of PO_4^{3-} was substituted by CO_3^{2-} in this apatite, while the concentration of Ca ions was maintained at a low level. As a result, the concentration of P ions in SBF increased because of the release of P ions from the DCPD coatings.

4 Conclusion

A bioactive calcium phosphate coating was prepared in a phosphating bath. By the investigation of morphology of coatings prepared on AZ91D magnesium alloy and acid drop test, we found that the optimal phosphating bath is composed of CaO=10 $g{\cdot}L^{-1}$, H_3PO_4 = 60 $mL{\cdot}L^{-1}$, $Ca(NO_3)_2$ = 10 $g{\cdot}L^{-1}$, Na_2MoO_4 = 1 $g{\cdot}L^{-1}$, $C_6H_4O_5NSNa$ = 1 $g{\cdot}L^{-1}$, pH = 3.0. XRD patterns show that the prepared coating is mainly composed of dicalcium phosphate dihydrate ($CaHPO_4{\cdot}2H_2O$, DCPD). The coating first is dissolved in SBF during the immersion test and then is mineralized. The appearance of carbonated hydroxyapatite indicates that the DCPD coating is bioactive and osteoconductive in SBF. A more positive potential and relatively lower anodic current density indicates that the DCPD coating on AZ91D magnesium alloy can evidently slow down the corrosion rate of the alloy in SBF, which is reflected by the decrease in the hydrogen evolution rate from 44.2 $mL{\cdot}cm^2{\cdot}d^{-1}$ of the bare magnesium alloy to 5.8 $mL{\cdot}cm^2{\cdot}d^{-1}$ of the magnesium alloy with DCPD coating.

Acknowledgment

This research was supported by the National Nature Science Foundation (No. 31070841), and the Foundation of National Key Basic Research and Development Program (No. 2010CB631001).

References

[1] Heublein B, Rohde R, Kaese V, Niemeyer M, Hartung W, Haverich A. Biocorrosion of magnesium alloys: A new principle in cardiovascular implant technology? *Heart*, 2003, **89**, 651–656.

[2] Witte F, Kaese V, Switzer H, Meyer-Lindenberg A, Wirth C J, Windhag H. *In vivo* corrosion of four magnesium alloys and the associated bone response. *Biomaterials*, 2005, **26**, 3557–3563.

[3] Witte F, Fischer J, Nellesen J, Crostack H, Kaese V, Pischd A, Beckmanne F, Windhagen H. *In vitro* and *in vivo* corrosion measurements of magnesium alloys. *Biomaterials*, 2006, **27**, 1013–1020.

[4] Gao J C, Wu S, Qiao L Y, Wang Y. Corrosion behavior of magnesium and its alloy in simulated body fluid. *The Journal of Clinical Rehabilitative Tissue Engineering Research*, 2007, **11**, 3584–3586.

[5] Xu L, Yu G, Zhang E, Pan F, Yang K. *In vivo* corrosion behavior of Mg–Mn–Zn alloy for bone implant application. *Journal of Biomedical Materials Research Part A*, 2007, **83**, 703–711.

[6] Song G L. Control of biodegradation of biocompatible magnesium alloys. *Corrosion Science*, 2007, **49**, 1696–1701.

[7] Gao J C, Wu S, Qiao L Y, Wang Y. Corrosion behavior of Mg and Mg-Zn alloys in simulated body fluid. *Transactions of Nonferrous Metals Society of China*, 2008, **18**, 588–592.

[8] Pietak A, Mahoney P, Dias G J, Staiger M P. Bone-like matrix formation on magnesium and magnesium alloys. *Journal of Materials Science Materials in Medicine*, 2008, **19**, 407–415.

[9] Li Z, Gu X, Lou S, Zheng Y. The development of binary Mg-Ca alloys for use as biodegradable materials within bone. *Biomaterials*, 2008, **29**, 1329–1344

[10] Vormann J. Magnesium: Nutrition and metabolism. *Molecular Aspects of Medicine*, 2003, **24**, 27–37.

[11] Ko Yeong-Mu, Lee Kang, Kim Byung-Hoon. Effect of Mg ion on formation of bone-like apatite on the plasma modified titanium surface. *Surface and Coatings Technology*, 2013, **228**, S404–S407.

[12] Maguire M E, Cowan J A. Magnesium chemistry and biochemistry. *Biometals*, 2002, **15**, 203–210.

[13] Okuma T. Magnesium and bone strength. *Nutrition*, 2001, **17**, 679–680.

[14] Rude R K, Gruber H E. Magnesium deficiency and osteoporosis animal and human observations. *Journal of Nutritional Biochemistry*, 2004, **15**, 710–716.

[15] Song G L. Control of biodegradation of biocompatable magnesium alloys. *Corrosion Science*, 2007, **49**, 1696–1701.

[16] Staiger M P, Pietak A M, Huadmai J, Dias G. Magnesium and its alloys as orthopedic biomaterials: A review. *Biomaterials*, 2006, **27**, 1728–1734.

[17] Wu F, Wei J, Guo H, Chen F P, Hong H, Liu C. Self-setting bioactive calcium-magnesium phosphate cement with high strength and degradability for bone regeneration. *Acta Biomaterialia*, 2008, **4**, 1873–1884.

[18] Liu G Y, Hu J, Ding Z K, Wang C. Bioactive calcium phosphate coating formed on micro-arc oxidized magnesium by chemical deposition. *Applied Surface Science*, 2011, **257**, 2051–2057.

[19] Wang Y, Wei M, Gao J C. Improve corrosion resistance of magnesium in simulated body fluid by dicalcium phosphate dihydrate coating. *Materials Science and Engineering C*, 2009, **29**, 1311–1316.

[20] Song Y, Zhang S X, Li J N, Zhao C L, Zhang X N. Electrodeposition of Ca-P coatings on biodegradable Mg alloy and *in vitro* biomineralization behaviors. *Acta Biomaterialia*, 2010, **6**, 1736–1742.

[21] Shi Y, Qi M, Chen Y, Shi P. MAO-DCPD composite coating on Mg alloy for degradable implant applications. *Materials Letters*, 2011, **65**, 2201–2204.

[22] Fulmer M T, Ison I C, Hankermayer C R, Constantz B R, Ross J. Measurements of the solubilities and dissolution rates of several hydroxyap-atites. *Biomaterials*, 2002, **23**, 751–755.

[23] Shi Z M, Song G L, Atrens A. The corrosion performance of anodised magnesium alloys. *Corrosion Science*, 2006, **48**, 3531–3546.

[24] Song Y W, Shang D Y, Chen R S, Han E H. Study on electroless Ni-P-ZrO_2 composite coatings on AZ91D magnesium alloys. *Surface Engineering*, 2007, **23**, 334–338.

[25] Lu X, Zhao Z F, Leng Y. Biomimetic calcium phosphate coatings on nitric-acidtreated titanium surfaces. *Materials Science and Engineering C*, 2007, **27**, 700–708.

[26] Pasinli A, Yuksel M, Celik E, Sener S, Tas A C. A new approach in biomimetic synthesis of calcium phosphate coatings using lactic acid-Na lactate buffered body fluid solution. *Acta Biomaterialia*, 2010, **6**, 2282–2288.

[27] Eppensteiner F W, Jenkins M R. Chromate conversion coatings. *Metal Finishing*, 2002, **100**, 479–491.

[28] Kwo Z C, Teng S S. Conversion-coating treatment for magnesium alloys by a permanganate–phosphate solution. *Materials Chemistry and Physics*, 2003, **80**, 191–200.

[29] Li G Y, Lian J S, Niu L Y, Jiang Z H. Influence of pH of phosphating bath on the zinc phosphate coating on AZ91D magnesium alloy. *Advanced Engineering Materials*, 2006, **8**, 123–127.

[30] Zhou W Q, Shan D Y, Han E H, Ke W. Structure and formation mechanism of phosphate conversion coating on die-cast AZ91D magnesium alloy. *Corrosion Science*, 2008, **50**, 329–337.

[31] Kouisni L, Azzi M, Zertoubi M, Dalard F, Maximovitch S. Phosphate coatings onmagnesium alloy AM60 part 1: Study of the formation and the growth of zinc phosphate films. *Surface and Coatings Technology*, 2004, **185**, 58–67.

[32] Cui X F, Li Y, Li Q F, Jin G, Ding M H, Wang F H. Influence of phytic acid concentration on performance of phytic acid conversion coatings on the AZ91D magnesium alloy. *Materials Chemistry and Physics*, 2008, **11**, 503–507.

[33] Dabala M, Brunelli K, Napolitani E, Magrini M. Cerium-based chemical conversion coating on AZ63 magnesium alloy. *Surface and Coatings Technology*, 2003, **172**, 227–232.

[34] Mhaede M, Pastorek F, Hadzima B. Influence of shot peening on corrosion properties of biocompatible magnesium alloy AZ31 coated by dicalcium phosphate dihydrate (DCPD). *Materials Science and Engineering C*, 2014, **39**, 330–335.

[35] Chang L, Tian L, Liu W, Duan X. Formation of dicalcium phosphate dihydrate on magnesium alloy by micro-arc oxidation coupled with hydrothermal treatment. *Corrosion Science*, 2013, **72**, 118–124.

[36] Hu J, Wang C, Ren W C, Zhang S, Liu F. Microstructure evolution and corrosion mechanism of dicalcium phosphate dihydrate coating on magnesium alloy in simulated body fluid. *Materials Chemistry and Physics*, 2010, **119**, 294–298.

[37] Xiao X, Zhu Q S, Su Y C, Li G Y. *In vitro* degradation and biocompatibility of Ca-P coated magnesium alloy. *Chemical Research in Chinese Universities*, 2013, **29**, 285–289.

[38] Gu X N, Zheng Y F, Chen L J. Influence of artificial biological fluid composition on the biocorrosion of potential orthopedic Mg-Ca, AZ31, AZ91 alloys. *Biomedical Materials*, 2009, **4**, 065011.

[39] Su Y C, Niu L Y, Lu Y B, Lian J S, Li G Y. Preparation and corrosion behavior of calcium phosphate and hydroxyapatite conversion coatings on AM60 magnesium alloy. *Journal of the Electrochemical Society*, 2013, **160**, 536–541.

[40] Tomozawa M, Hiromoto S. Microstructure of hydroxyapatite- and octacalcium phosphate-coatings formed on magnesium by a hydrothermal treatment at various pH values. *Acta Materialia*, 2011, **59**, 355–363.

[41] Song Y W, Shan D Y, Han E H. Electrodeposition of hydroxyapatite coating on AZ91D magnesium alloy for biomaterial application. *Materials Letter*, 2008, **62**, 3276–3279.

[42] Wang H X, Guan S K, Wang X, Ren C X, Wang L G. *In vitro* degradation and mechanical integrity of Mg-Zn-Ca alloy coated with Ca-deficient hydroxyapatite by the pulse

electrodeposition process. *Acta Biomaterialia*, 2010, **6**, 1743–1748.

[43] Song G, Atrens A. Corrosion mechanisms of magnesium alloys. *Advanced Engineering Materials*, 1991, **1**, 11–33.

[44] Song G, Atrens A. Understanding magnesium corrosion-a framework for improved alloy performance. *Advanced Engineering Materials*, 2003, **5**, 837–857.

[45] Song G. Recent progress in corrosion and protection of magnesium alloys. *Advanced Engineering Materials*, 2005, **7**, 563–586.

[46] Song G, St John D. The effect of zirconium grain refinement on the corrosion behaviour of magnesium rare earth alloy MEZ. *Journal of Light Metals*, 2002, **2**, 1–16.

[47] Song G, Atrens A, St John D. *Magnesium technology* 2001. In Hryn J N ed., *Proceeding of the symposium held during TMS Annual Meeting*, New Orleans, LA, TMS, 2001, 255–262.

[48] Zhang Q, Chen J, Feng J, Cao Y, Deng C, Zhang X. The dissolution and mineralization behaviors of HA coatings. *Biomaterials*, 2003, **24**, 4741–4748.

[49] Lee K Y, Park M, Kim H M, Lim Y J, Chun H J, Kim H, Moon S H. Ceramic bioactivity: Progresses, challenges and perspectives. *Biomedical Materials*, 2006, **1**, R31–R37.

[50] Tanahashi M, Matsuda T J. Surface functional group dependence on apatite formation on self-assembled monolayers in a simulated body fluid. *Journal of Biomedical Materials Research*, 1997, **34**, 305–315.

[51] Bertazzo S, Bertran C A. Morphological and dimensional characteristics of bone mineral crystals. *Key Engineering Materials*, 2006, **309**–**311**, 3–10.

[52] Legros R, Balmain N, Bonel G. Age-related changes in mineral of rat and bovine cortical bone. *Calcified Tissue International*, 1987, **41**, 137–144.